EFFECT OF TEMPERATURE AND TIME ON MICROSTRUCTURE AND SURFACE FUNCTIONAL GROUPS OF ACTIVATED CARBON FIBERS PREPARED FROM LIQUEFIED WOOD

Wenjing Liu and Guangjie Zhao *

Activated carbon fibers were prepared from liquefied wood through stream activation. The effects of activation temperature and time on the microstructure and surface functional groups of the liquefied wood activated carbon fibers (LWACFs) were studied using analysis of burning behavior, X-ray diffraction, nitrogen adsorption-desorption isotherms, X-ray photoelectron spectroscopy, and SEM. The results showed that the burn-off value of the LWACFs increased gradually with the increase in temperature or time. All the LWACFs were far from being structurally graphitized, and in general, as temperature or time increased, the degree of graphitization and thickness of crystal structure increased. In addition, the LWACFs possessed rich micropores, and their specific surface area, pore volume, micropore size, and mesopore quantity were directly related to the activation temperature or time. The maximum specific surface area was found to be 2641 m^2/g. The fractal dimension values of all samples were close to 3, indicating that their surfaces were very rough. Furthermore, with an increase in temperature or time, the elemental content of carbon increased, while that of oxygen decreased. Meanwhile, as the temperature or time increased, the relative content of graphitic carbon decreased, whereas that of carbon bonded to oxygen-containing functions increased. The surface of samples prepared at higher temperature or with longer time formed a considerable amount of holes.

Keywords: Wood resource; Activated carbon fiber; Microstructure; Surface functional groups

*Contact information: a: College of Material Science and Technology, Beijing Forestry University, Beijing 100083 China; *Corresponding author: zhaows@bjfu.edu.cn*

INTRODUCTION

Activated carbon fibers (ACFs) are widely applied in many fields, where they are used for adsorption and separation, catalyst support, electronic materials, and the storage of natural gas materials due to their abundantly developed pore structure and special surface reactivity (Shen *et al.* 2006). ACFs can be produced from polyacrylonitrile (PAN) fibers, pitch fibers, phenolic fibers, cellulose fibers, *etc*. Meanwhile, environmental protection and resource conservation have attracted more and more attention in recent years. There has been a resurgence of interest in using the abundant and renewable biomass resources as an alternative to petrochemical resources (Xu and Etcheverry 2008). Therefore, wood, as a main component of biomass, is being put to use in the production of wood activated carbon fibers (WACFs). WACFs, with wood as a raw material, have the potential to not only reduce production costs but also to achieve the aim of sustainable development and effective utilization of woody biomass components (Uraki *et al.* 2001).

The study of WACFs can be traced back to the middle of last century. In 1962, Abbott successfully developed viscose-based ACFs. Ten years later, Arons and Lin published their research on viscose-based activated carbon fibers (see Arons and Macnair 1972). Notably, these different precursors gave rise to final products having different properties. WACFs have many advantages, such as high yield, large surface area, and great static adsorption capacities (Fu *et al.* 2003). Uraki *et al.* (2001) studied ACFs from softwood acetic acid lignin, and the results showed that as the activation time increased, the yield decreased and the surface area increased markedly. Ishii *et al.* systematically investigated the structure of pitch and cellulose-based ACFs and found that both the stacking height and stacking width of the ACFs increased remarkably as temperature increased, and also that the cellulose-based ACFs were richer in pore structure than the pitch-based ACFs (Ishii *et al.* 1997; Uraki *et al.* 2001).

As previously reported, the cellulose and lignin of wood have been used as raw materials to produce WACFs (Ishii *et al.* 1997; Polovina *et al.* 1997; Uraki *et al.* 2001). However, in this study, a new method was applied: liquefied wood was utilized to produce liquefied wood activated carbon fibers (LWACFs). Compared with previous preparation methods for WACFs such as lignin activated carbon fibers (LACFs), this method did not require the separation of some components from the wood, so actual wood utilization was greater than it would be using other methods. Essentially, the wood liquefaction technique was designed to convert wood into liquid material using polyethylene glycol and phenols (Alma *et al.* 1995). Liquefied wood had been used previously to prepare adhesives (Alma *et al.* 2001), foam (Wang *et al.* 2012), wood ceramics (Hirose *et al.* 2002), carbon fibers (Ma and Zhao 2010), and so on. However, few studies on activated carbon fibers prepared from wood liquefied with phenols have been reported.

In this study, LWACFs were prepared through liquefaction, spinning, curing, carbonization, and the activation processes. Notably, carbonization and activation were completed in a single step in order to reduce energy consumption. In addition, the microstructure and surface functional groups of the liquefied wooden activated carbon fibers were investigated, and their investigation was helpful in optimizing the technical parameters. Moreover, the adsorption of carbonaceous adsorbents was dependent on the microstructure and surface chemistry. Therefore, the aim of the present work was to explore a new and effective adsorbent carbon material prepared from biomass that could be widely applied in the interests of environmental protection, the chemical industry, the production of electronics, and various other fields.

EXPERIMENTAL

Materials

Wood flour (*Cunninghamia lanceolata*) was mixed with phenols containing 10 wt% H_3PO_4 as the active catalyst. The wood/phenol ratio was 1/5 by weight. The mixture was liquefied by means of stirring at 160 ^oC for 2.5 hours. After the liquefaction of the wood, 5 wt% hexamethylenetetramine, to be used as a synthesis agent, was added to the liquefied wood, all of which was then heated to 170 ^oC in a period of 40 min and held for 10 min to prepare the spinning solution.

The as-spun fibers were prepared by means of fusion spinning at 120 ^oC with a laboratory spinning apparatus. When the fusion spinning was completed, the as-spun

fibers were cured via soaking in an acid solution with HCHO and HCl (1:1 by volume) as the main components at 85 °C for 2 hours, a process for the production of precursors that was designed in accordance with predetermined technical parameters (Ma and Zhao 2008, 2010, 2011). The precursors were then washed with deionized water and finally dried at 90 °C for 4 hours.

The precursors were carbonized and activated at temperatures between 700 and 900 °C for periods of time between 10 and 90 min by introducing steam mixed with nitrogen in one step. Those samples treated at different conditions were denoted by temperature-time codes, such as 700-60.

Methods

The burn-off (%), as an index of weight loss, indicating the degree of carbonization and activation, was calculated as follows,

$$\text{Burn-off} = (w_1\text{-}w_2)/\ w_1 \times 100 \quad (1)$$

where w_1 and w_2 are the weight of the precursor fibers and activated carbon fibers, respectively.

The X-ray diffraction (SHIMADZU, XRD-6000) measurements were conducted with an X-ray diffractometer using CuKa radiation (wavelength 0.154nm) at 40 kV and 30 mA. The scanning rate was 2°/min with a scanning step of 0.2° from 5° to 60° (2θ). The value of lamellar spacing (d_{002}) was calculated using Bragg's law, and the lattice size (L_c) along the c-axis direction was calculated from the Scherrer's formula,

$$d_{002}=\frac{\lambda}{2\sin\theta} \quad (2)$$

$$L_c=\frac{k\lambda}{\beta\cos\theta} \quad (3)$$

where 2θ is the scattering angle, λ is the wavelength of the X-ray used, and β is the full width at half the maximum intensity (FWHM). The form factor k is 0.89 (Ma and Zhao 2011).

Nitrogen adsorption isotherms were measured using a Surface Area Analyzer and a Pore Size Analyzer: Autosorb-iQ (Quantachrome Instruments Corporate). All samples were out-gassed at 300 °C for 3 hours before measurement. The specific surface area (S_{BET}) of the ACF was calculated from nitrogen adsorption using the BET equation (Brunauer *et al.* 1938). The micropore volume (V_{micro}) and micropore area (S_{micro}) were estimated using the *t*-plot micropore method (de Boer *et al.* 1966). The pore volume (V_{total}) and diameter were based on the assumption that nitrogen filled the sample pores at a relative pressure of 0.995. The pore size distribution was determined according to the density functional theory (DFT) (Lastoskie *et al.* 1993). Surface roughness is an important factor that has influence on the adsorption property of an adsorbent. The fractal dimension, a measure of the roughness of a surface, was determined from the nitrogen adsorption isotherms on the LWACF samples using the FHH (Frenkel-Halsey-Hill) equation for nitrogen adsorption isotherms (Hayashi *et al.* 2002).

X-ray photoelectron spectroscopy (XPS), which is also referred to as Electron Spectroscopy for Chemical Analysis (ESCA), was used to determine the number and type of functional groups present on the surface of the LWACFs. The XPS spectra of all

samples were obtained using a spectrophotometer (Thermo Scientific ESCALAB 250Xi). A monochromatic AlK α X-ray (1486.6 eV) source was used for this analysis. The survey scans were collected from the binding energy range of 0 to 1350 eV. The spectral deconvolution was conducted using the XPSPEAK software. A Shirley type background was chosen to be subtracted prior to quantification. After the baseline was subtracted, the curve-fitting was performed using an asymmetric Gaussian–Lorentzian sum function fitting program under an optimized peak shape. This peak-fitting procedure was iterated until an acceptable fit was obtained.

The surface morphology of LWACFs was examined with a scanning electron microscope (SEM, S-3000N, Hitach Company in Japan). Before observation, the samples were metalized with a thin layer of Pt.

RESULTS AND DISCUSSION

Burning Behavior

Figure 1 presents the burn-off results for the LWACF samples. As seen from the data, the burn-off values increased gradually with increases in temperature or time, finally reaching a loss of 90 wt% at the temperature of 900 °C for 60 min or reaching a loss of 71 wt% when the temperature was held at 800 °C after activation for 90 min. This indicated that increasing numbers of non-carbon atoms were being released from the samples as the temperature or time increased. However, as shown in Fig. 1, the maximum derivative mass losses for the LWACF samples took place at temperatures ranging from 800 to 850 °C or after times between 60 and 90 min, illustrating that these periods formed the key activation reaction stage for the LWACFs.

Crystal Structure

The X-ray diffraction (XRD) patterns of the LWACFs are shown in Fig. 2. The figure shows that 2θ had two graphitic diffraction peaks at 23° and 44°, which were assigned to the disordered graphitic 002 plane and the 10 plane (overlapped 100 and 101), respectively (Ryu *et al.* 2002). Though the profiles of the LWACFs activated with various processes were very similar, some slight differences can be observed in Fig. 2(a). That is, as the temperature was increased, the 002 peaks at 23 ° became broader, while the 10 peaks at 44 ° became sharper.

The structural parameters for the samples investigated are given in Table 1. Generally speaking, the value of the interlayer spacing (d) can be used to evaluate the degree of graphitization of the carbon materials. A larger stacking height (L_c) suggests a thicker graphite-like structural layer, and a higher average carbon layer (L_c/d) further implies a denser structure (Su *et al.* 2012). As listed in Table 1, the value of d was between 0.359 nm and 0.403 nm, which was much higher than the ideal graphite spacing (0.335 nm) would be, demonstrating that all the LWACFs were far from having a graphitized structure. From 700 °C to 800 °C, d, L_c, L_c/d, and the crystallinity were not much affected by the temperature. However, when the temperature first exceeded 800 °C, d decreased and then increased as the temperature continued to rise, whereas L_c, crystallinity, and L_c/d showed a tendency contrary to that of d. This reflected that the structure of the fibers changed gradually from an aromatic structure into a graphitic structure within the temperature range of 700 °C to 800 °C, and that when the temperature exceeded 800 °C, the graphite crystallites kept on growing and forming a denser and

thicker graphite-like structure as a result. Nevertheless, this graphite-like structure was broken at 900 °C due to the strengthened activation reaction.

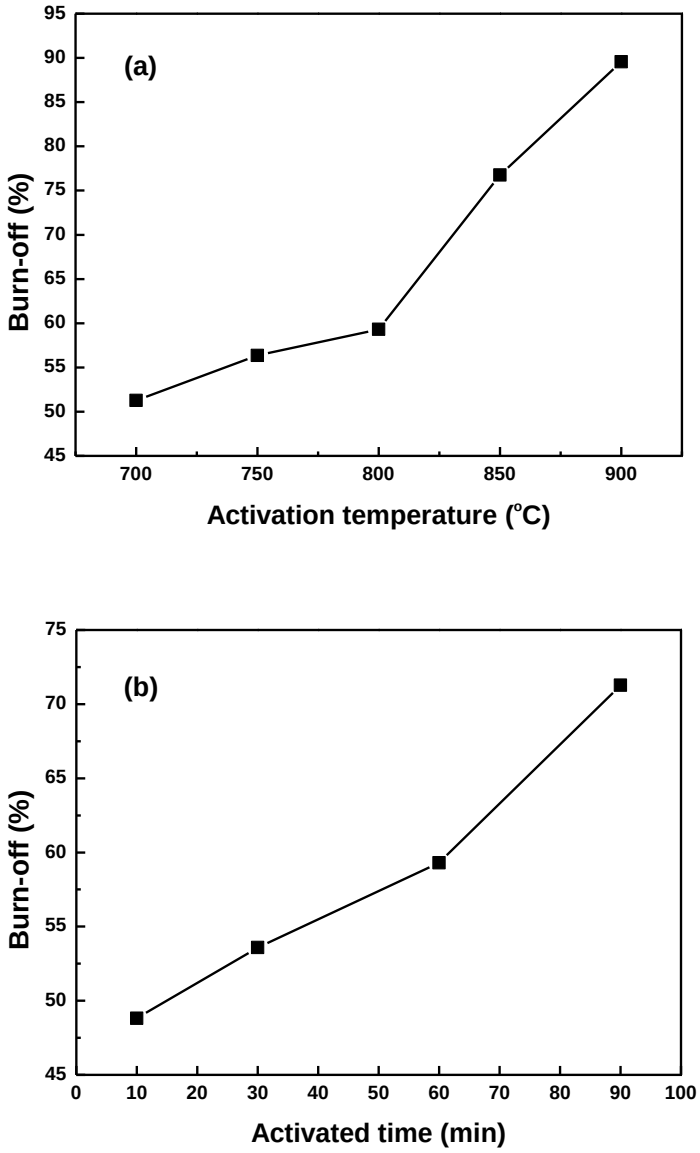

Fig. 1. Burn-off of the LWACF samples: (a) Effect of different temperatures for 60 min; (b) Effect of different times at 800 °C

As time proceeded, the interlayer spacing (*d*) also decreased initially and then increased. This indicated that a well-chosen increase in time could improve the degree of graphitization, although the activation reaction could damage the graphite-like structure if the time reached 90 min. On the other hand, L_c, L_c/d, and crystallinity increased more markedly at the time of 90 min than at other activation times. This suggested that the thicker crystals and denser structure were formed by long-time treatment.

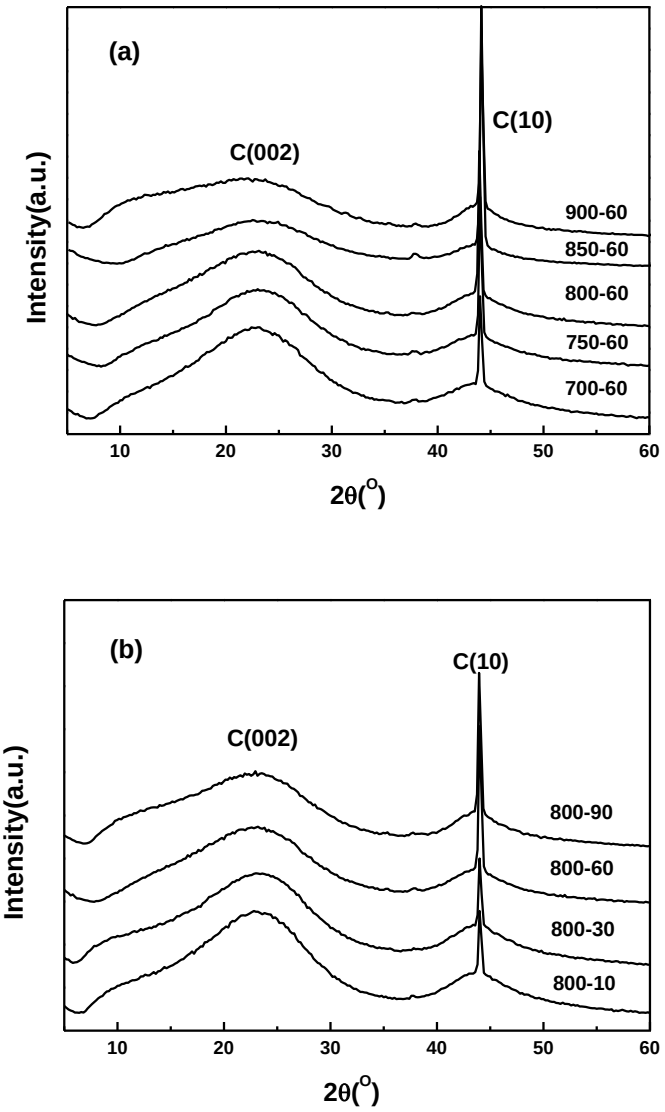

Fig. 2. X-ray diffraction patterns of the LWACFs: (a) Effect of different temperatures for 60 min; (b) Effect of different times at 800 ^{o}C

Table 1. Structural Parameters of Graphite-like Crystallite in the LWACFs

Sample	d_{002} (nm)	Lc (nm)	Lc/ d_{002}	Crystallinity (%)
700-60	0.386	0.147	0.380	25.259
750-60	0.387	0.141	0.364	28.666
800-60	0.383	0.167	0.436	28.658
850-60	0.359	0.369	1.028	36.798
900-60	0.376	0.314	0.835	31.014
800-10	0.390	0.178	0.457	25.941
800-30	0.386	0.115	0.297	25.940
800-90	0.403	0.299	0.742	28.685

Pore Structure

The nitrogen adsorption-desorption isotherms of LWACFs are shown in Fig. 3. According to the IUPAC classification, the type of adsorption curve belongs to Type Ⅰ, which is indicative of the presence of micropores. The amount of adsorption increased remarkably with increasing temperature or time, which indicated that more pores were being formed at higher temperatures or after longer periods of time. Moreover, when the temperature reached 850 to 900 °C or the time reached 90 min, the "knee" of isotherms appeared more round at low relative pressures, which is normally associated with wide micropores. At a relative pressure of about 0.2, the amount of adsorption still increased with the increase in relative pressure, which is indicative of a certain volume of mesopores in all the samples (Lee *et al.* 2006).

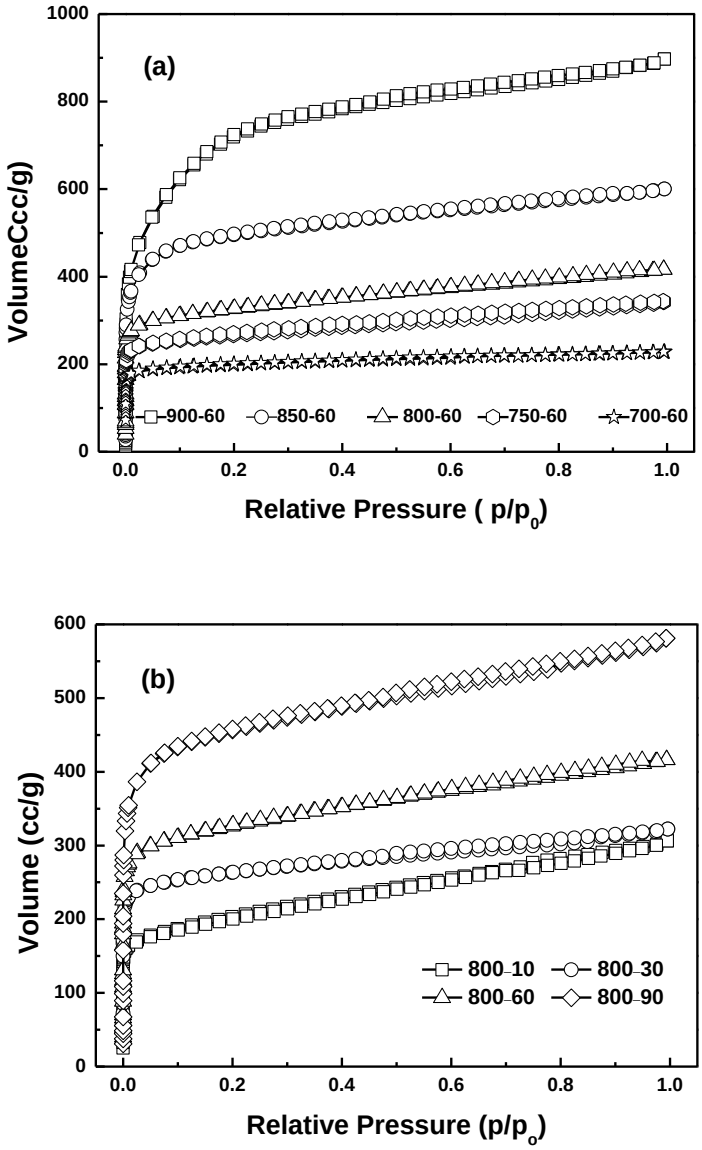

Fig. 3. Nitrogen adsorption-desorption isotherm of LWACFs: (a) Effect of different temperatures for 60 min; (b) Effect of different times at 800 °C

The pore characteristics of the LWACF samples are summarized in Table 2. The table shows that the maximum BET specific surface area was 2641 m^2/g, which was comparable to that of high-grade commercial ACFs (Uraki *et al.* 2001). Moreover, according to previous research, the surface area of lignin-ACF is approximately 2000 m^2/g, and that of PAN-ACF and rayon-based ACF is about 1500 m^2/g (Chiang *et al.* 2007; Lee *et al.* 2006; Uraki *et al.* 2001). The table also showed that the total pore volume of the samples varied from 0.353 cm^3/g to 1.388 cm^3/g. Meanwhile, the specific surface area (S_{BET}, S_{micro}, and S_{meso}) and pore volume (V_{total}, V_{micro}, and V_{meso}) of LWACFs followed an increasing trend with the increase in temperature. The results indicated that stream molecules could react more quickly with active amorphous atoms and unsaturated carbon atoms to form more numerous pores, gaps, and cracks with the increase in temperature, thus increasing the specific surface area and pore volume in unit weight (Su *et al.* 2012). In addition, S_{micro} and V_{micro} had much higher values than did S_{meso} and V_{meso} for all samples, which suggested that the high specific surface area and pore volume were due to an abundance of micropores present in the LWACFs. As for the average pore diameter of the samples, which was distributed from 1.800 nm to 2.102 nm, this changed slightly with the variation of temperature.

Table 2. Pore Characteristics of LWACF Samples by Nitrogen Adsorption Isotherms

Sample	Specific Surface Area (m^2/g)			Pore Volume (cm^3/g)			Average Pore diameter(nm)	Micropore Ratio (%)	Fractal Dimensions	
	S_{BET}	S_{micro}	S_{meso}	V_{total}	V_{micro}	V_{meso}	d	V_{micro}/V_{total}	D_1[a]	D_2[b]
700-60	784.	692	92	0.353	0.269	0.084	1.800	76.204	2.783	2.928
750-60	1029	825	203	0.530	0.325	0.205	2.058	61.321	2.646	2.882
800-60	1249	968	281	0.644	0.384	0.260	2.062	59.627	2.606	2.869
850-60	1882	1560	322	0.928	0.629	0.299	1.974	67.780	2.699	2.900
900-60	2641	2092	549	1.388	0.898	0.490	2.102	64.697	2.655	2.885
800-10	740	449	291	0.474	0.190	0.284	2.558	40.084	2.365	2.788
800-30	1021	864	157	0.498	0.341	0.157	1.952	68.474	2.721	2.907
800-90	1737	1388	349	0.899	0.556	0.343	2.070	61.846	2.651	2.884

a: $D_1$was obtained by neglecting adsorbate surface tension effects.
b: $D_2$was obtained by accounting for adsorbate surface tension effects.

As the time increased, the specific surface area (S_{BET} and S_{micro}) and pore volume (V_{total} and V_{micro}) of the LWACFs increased. This was because initially during the process of activation, only the amorphous carbon was burned away, but at further stages of activation, even the intercrystalline layers could be burned away. Therefore, as time passed, the carbon atoms at the intercrystalline layers reacted with atoms within the steam to form numerous pores, gaps, and cracks, thus increasing the pore specific surface area in unit weight (Grebennikov and Fridman 1988). As for mesopores, their ratio in the samples treated for 10 min was much higher than that of the other samples, and their average pore diameter was the largest, about 2.558 nm. The reason for this was that the samples had not become fully carbonized earlier, resulting in a partially graphite-like structure with larger interlayer spacing. However, as time passed, there was moderate

shrinkage of the structure, and thus the pores became much narrower (Mangun *et al.* 2001).

It can be seen from Table 2 that S_{BET} values for some samples were similar to each other, such as the values for 700-60 and 800-10, 750-60 and 800-30, and 800-90 and 850-60. This demonstrated that a high S_{BET} value could be obtained by two methods, *i.e.*, increasing the temperature or increasing the time, depending on the actual requirements of production. As shown in Table 2, the fractal dimensions values of the LWACF samples were between 2.6 and 2.8, so, close to 3, indicating that their surfaces were very rough. The different treatments had little effect on the fractal dimensions. In addition, it could also be concluded that fractal dimension was inversely related to micropore distribution.

Figure 4 shows the pore size distributions, based on the DFT, of the LWACF samples. It can be seen in this figure that the samples took on a narrow pore size distribution, and that their pore sizes were mainly distributed between 0.5 and 2 nm, placing them as belonging to the micropore structure.

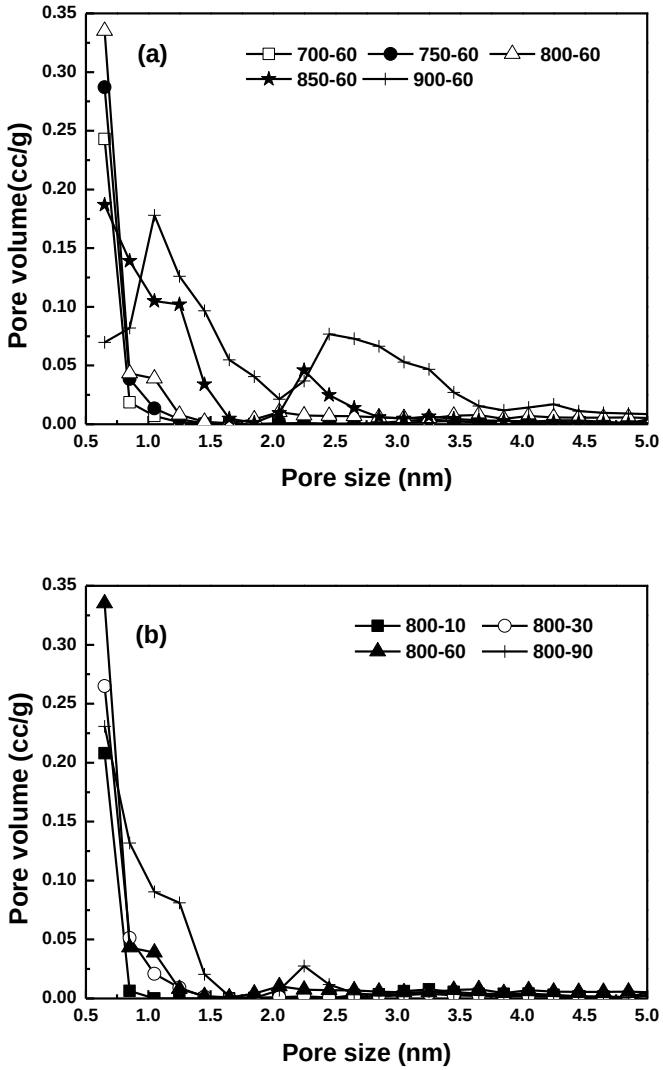

Fig. 4. Pore size distributions of the LWACF samples: (a) Effect of different temperatures for 60 min; (b) Effect of different times at 800 ^{o}C

In Fig. 4(a), the micropore size is seen to have generally increased when the temperature was increased. This was because the high temperature treatment had removed the active amorphous atoms and unsaturated carbon atoms from the edges of the micrographitic walls and partially gasified the micropore walls, thereby increasing the size of the micropores (Ishii *et al.* 1997). Meanwhile, when the temperature rose to 850 and 900 ^{o}C, there were peaks at the pore size of 2.0 to 3.0 nm, respectively, which suggested that more mesopores were produced. As can be seen in Fig. 4(b), the micropore size became larger with the increase in time as well, and more mesopores appeared as time increased. This expansion of the size of the micropores was attributed to the risk that carbon molecules at intercrystallite layers might be burned away at later stages of activation.

Surface Functional Groups

Figure 5 shows the XPS spectra of LWACFs.

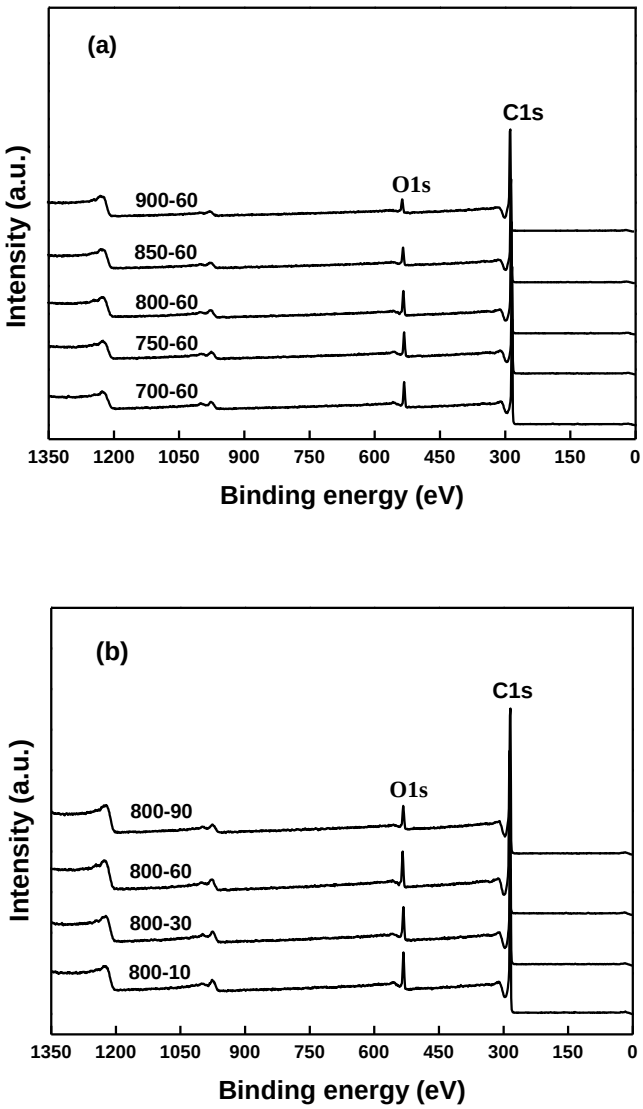

Fig. 5. XPS spectra of the LWACF samples: (a) Effect of different temperatures for 60 min; (b) Effect of different times at 800 ^{o}C

As shown in the figure, the elements C and O were the basic elements of the LWACFs. With the increase in temperature or time, the peak of element C grew, while that of oxygen dropped. The main elemental composition of the surface of the LWACF samples is shown in Table 3. As can be seen from the table, carbon was the most abundant constituent in all of the LWACF samples. The samples prepared at higher temperatures or for longer periods of time possessed more carbon and less of the elements O or N. This indicated that significantly more surface oxides were removed as temperature or time increased.

Table 3. Elemental Composition of the Surface of LWACFs (at %)

Sample	C1s	O1s	N1s	[O]/[C] (%)	[N]/[C] (%)
700-60	89.41	10.23	0.36	11.44	0. 40
750-60	90.14	9.39	0.47	10.42	0.52
800-60	90.79	8.89	0.32	9.79	0.35
850-60	92.52	7.15	0.33	7.73	0.36
900-60	94.02	5.72	0.26	6.08	0.28
800-10	89.46	10.13	0.42	11.32	0.47
800-30	90.27	9.39	0.33	10.40	0.36
800-90	92.37	7.34	0.29	7.94	0.31

In order to obtain information about the chemical composition of the fiber surface and the binding characteristics of the elements at the surface, measurements of the XPS spectra of the C1s region were analyzed. The C1s spectra of the eight samples were almost the same, so only the 700-60 sample is shown in Fig. 6 as an example. As in the figure, the spectra of the C1s region exhibited an asymmetric tailing, which was partially due to the intrinsic asymmetry of the graphite peak or to the contribution of oxygen surface complexes. Curve fitting was optimized into five peaks: the graphitic carbon (BE = 284.7 eV), the carbon present in phenolic, alcohol, ether, or C = N groups (BE = 285.5 eV), carbonyl or quinine groups (BE = 286.8-286.9 eV), carboxyl or ester groups (BE = 288.8-289.1 eV), and carbonate groups (BE = 290.8-291.1 eV) (Chiang *et al.* 2007).

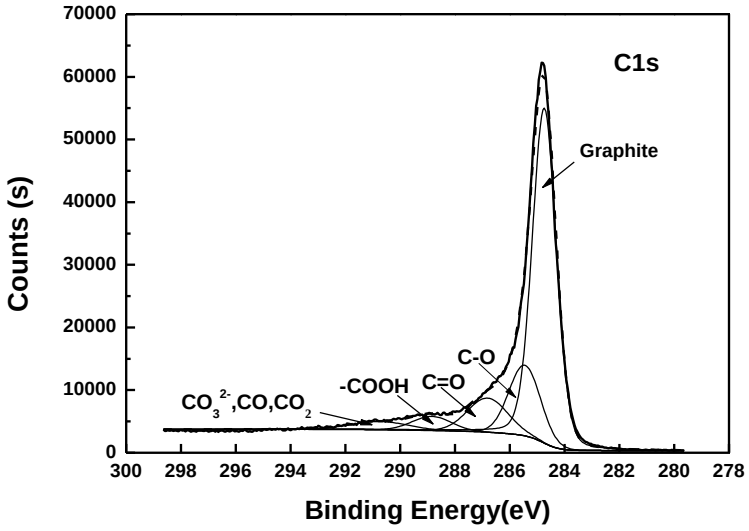

Fig. 6. XPS spectra of C1s region of the LWACFs

The results for the fits of the C1s region are listed in Table 4. It can be seen in the table that the relative content of the graphitic carbon decreased as the temperature or time increased, whereas that of the carbon bonded to oxygen-containing functions changed according to the opposite trend. It is believed that more graphitic carbon could react with stream molecules to generate the carbon bonded to oxygen-containing functions as the temperature or time increased. Aside from the graphitic carbon, C-O groups were the predominant function on the surface of the LWACFs. The relative composition of the fibers' surface was similar to that of published data (Paiva *et al.* 2000; Park *et al.* 2003). In addition, the relative content of the carbonyl and carbonate groups was generally positively correlated with temperature or time.

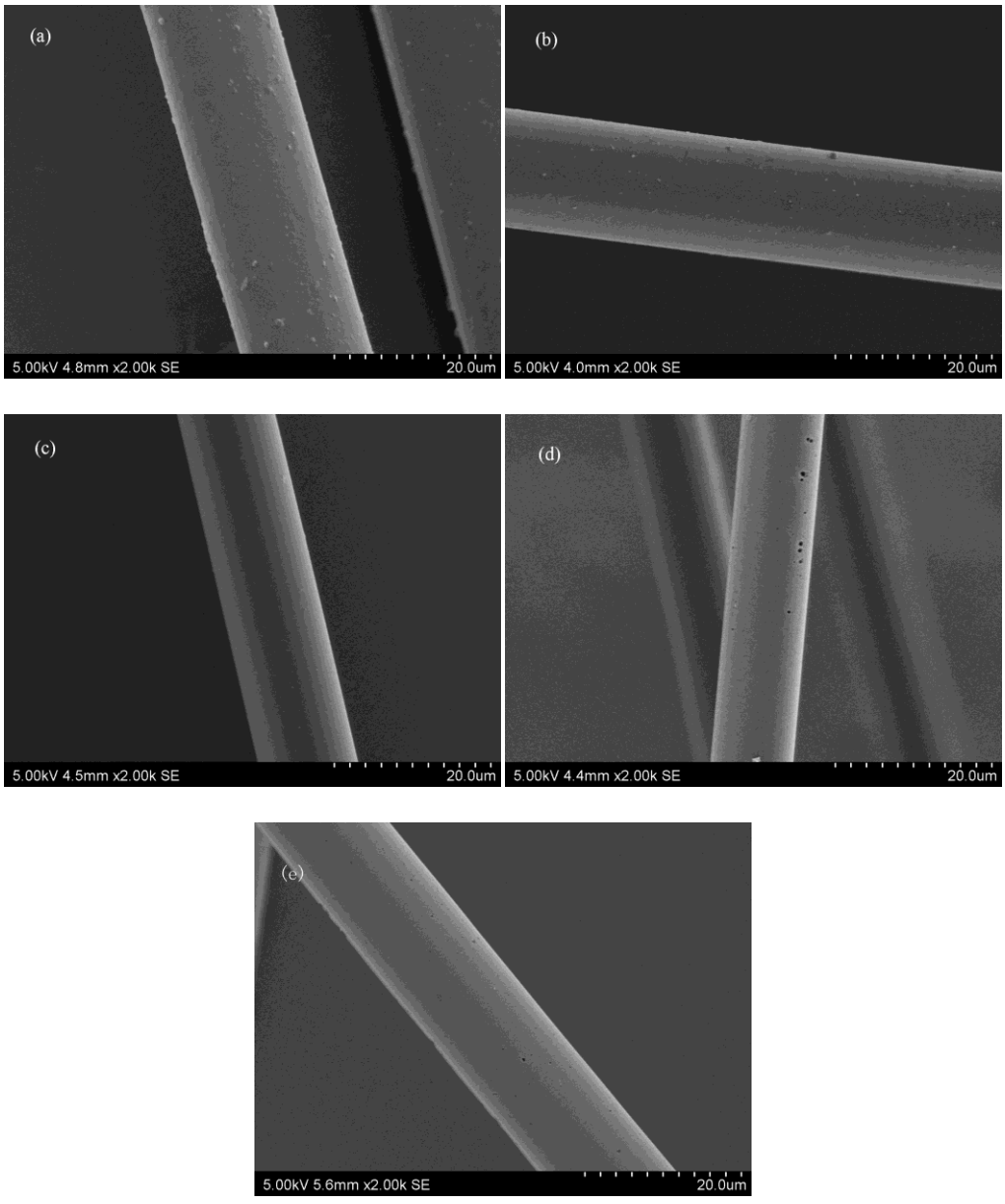

Fig. 7. SEM images of the LWACF samples with different temperatures: (a) 700-60, (b) 750-60, (c) 800-60, (d) 850-60 and (e) 900-60

Table 4. Results of the Fits of the C1s Region

Sample	Graphite (%)	C-O (%)	C=O (%)	-COOH (%)	CO_3^{2-},CO,CO_2 (%)
	284.7 (eV)	285.5 -285.9 (eV)	286.8 -287.1 (eV)	288.8 -289.1 (eV)	290.8- 291.4 (eV)
700-60	65.16	16.93	10.29	4.15	3.47
750-60	65.37	16.88	10.25	3.94	3.56
800-60	64.11	14.89	9.88	5.91	5.21
850-60	62.21	15.44	10.11	5.04	7.08
900-60	60.43	15.81	10.56	5.36	7.83
800-10	68.11	13.07	9.11	5.42	4.29
800-30	65.82	12.71	9.66	6.30	5.50
800-90	61.75	13.38	10.07	5.29	9.52

Surface Morphology

SEM micrographs of the LWACF samples prepared at different temperatures are presented in Fig. 7. When the temperature was 700, 750, or 800 ^{o}C, the surface of samples was smooth. However, when the temperature was heated to 850 or 900 ^{o}C, a considerable amount of holes were observed on the surface of these samples. Figure 8 shows SEM images of the LWACF samples for different times. The surface was smooth for periods of time between 10 and 60 min. When the time was prolonged to 90 min, there were numerous holes on the samples' surface. These results reveal that activation effect on the fibers could be strengthened with an increase in temperature or time; thus the holes were formed by destruction of the walls between some pores.

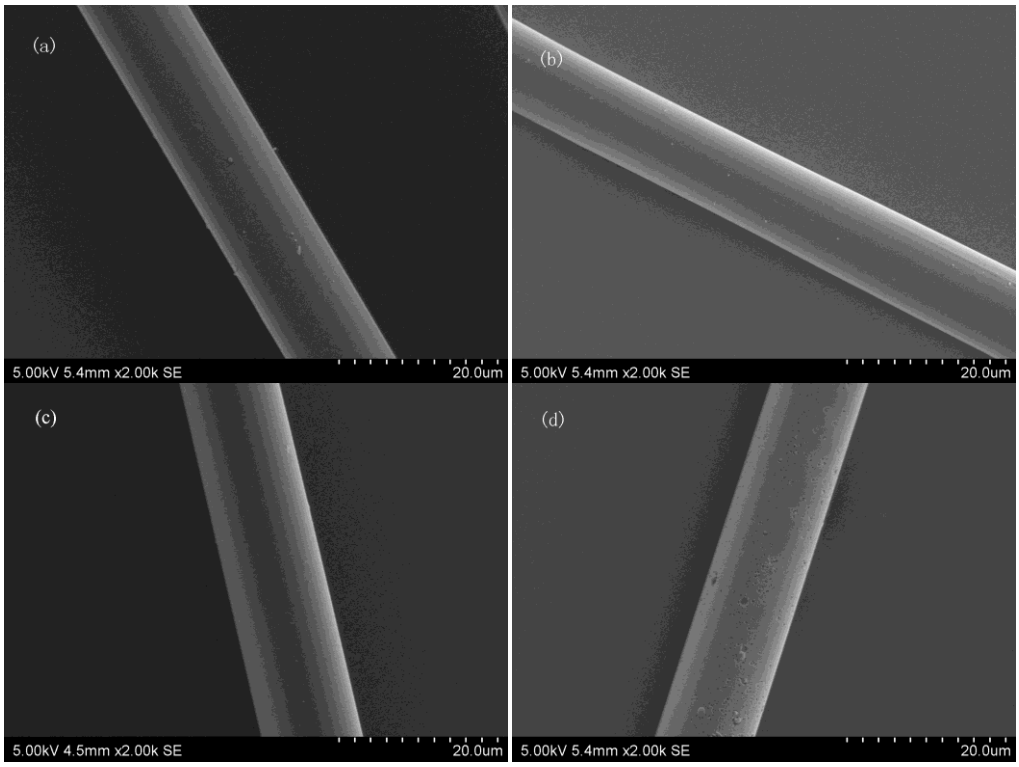

Fig. 8. SEM images of the LWACF samples with different times: (a) 800-10, (b) 800-30, (c) 800-60, and (d) 800-90

CONCLUSIONS

1. Liquefied wood activated carbon fibers (LWACFs) were prepared from liquefied wood through stream activation. The burn-off value of the LWACF samples increased gradually with increasing temperature or time, finally reaching a loss of 90 wt% at the temperature of 900 °C when the time of activation was 60 min or showing a loss of 71 wt% after activation of 90 min when the temperature held on 800 °C. Temperatures ranging from 800 to 850 °C or times between 60 and 90 min were the key activation reaction stage for the LWACFs
2. All LWACFs were far from being structurally graphitized. In general, as temperature or time increased, the degree of graphitization and thickness of the crystal structure increased. The structure of the fibers changed gradually from the aromatic structure into the graphite structure within the temperature range of 700 °C to 800 °C. When the temperature exceeded 800 °C, the graphite crystallites kept on growing and forming a denser and thicker graphite-like structure as a result. However, the activation reaction could damage the graphite-like structure if the temperature reached 900 °C or the time was prolonged to 90 min.
3. The nitrogen adsorption-desorption isotherms of LWACFs all belonged to Type I. This indicated the presence of micropores. The specific surface area (S_{BET}, S_{micro}, and S_{meso}) and pore volume (V_{total}, V_{micro}, and V_{meso}) of the LWACF samples increased with the increase in temperature or time, and the maximum specific surface area was found to be 2641 m^2/g. In addition, the size of micropores and the quantity of mesopores both increased as temperature or time increased. The fractal dimension values of all of the LWACF samples were close to 3, indicating that their surfaces were very rough. The different treatments had little effect on the fractal dimensions.
4. Carbon was the most abundant elemental constituent of all the LWACFs. As the temperature or time was increased, the amount of carbon increased and the amount of oxygen decreased. Meanwhile, as temperature or time increased, the relative content of graphitic carbon decreased, whereas that of carbon bonded to oxygen-containing functions increased. Moreover, the C-O groups were the predominant function on the surface of the LWACFs. The relative content of carbonyl and carbonate groups was generally positively correlated with temperature or time.
5. When the samples were heated above 850 °C or the time was prolonged to 90 min, a considerable amount of holes were observed on the surface of samples. These results reveal that activation effect on the fibers could be strengthened with an increase in temperature or time; thus the holes were formed by destruction of the walls between some pores.

ACKNOWLEDGMENTS

The authors are grateful for the support of the Special Research Funds of Forestry Industry for Public Welfare of China, Grant. No. 201004057.

REFERENCES CITED

Alma, M. H., Batìrk, M. A., and Shiraishi, N. (2001). "Cocondensation of NaOH-Catalyzed Liquefied Wood Wastes, Phenol, and Formaldehyde for the Production of Resol-Type Adhesives," *Industrial & Engineering Chemistry Research* 40(22), 5036-5039.

Alma, M., Yoshioka, M., Yao, Y., and Shiraishi, N. (1995). "Preparation and characterization of the phenolated wood using hydrochloric acid (HCl) as a catalyst," *Wood Science and Technology* 30(1), 39-47.

Arons, G. N., and Macnair, R. N. (1972). "Activated carbon fiber and fabric achieved by pyrolysis and activation of phenolic precursors," *Textile Research Journal* 42(1), 60 - 63.

Brunauer, S., Emmett, P. H., and Teller, E. (1938). "Adsorption of gases in multimolecular layers," *Journal of the American Chemical Society* 60(2), 309-319.

Chiang, Y., Lee, C., and Lee, H. (2007). "Characterization of microstructure and surface properties of heat-treated PAN-and rayon-based activated carbon fibers," *Journal of Porous Materials* 14(2), 227-237.

de Boer, J. H., Lippens, B. C., Linsen, B. G., Broekhoff, J. C. P., van den Heuvel, A., and Osinga, T. J. (1966). "T-curve of multimolecular N_2-adsorption," *Journal of Colloid and Interface Science* 21(4), 405-414.

Fu, R., Liu, L., Huang, W., and Sun, P. (2003). "Studies on the structure of activated carbon fibers activated by phosphoric acid," *Journal of Applied Polymer Science* 87(14), 2253-2261.

Grebennikov, S. F., and Fridman, L. I. (1988). "Microstructure of activated carbon fibres," *Fibre Chemistry* 19(6), 385-389.

Hayashi, J. I., Muroyama, K., Gomes, V. G., and Watkinson, A. P. (2002). "Fractal dimensions of activated carbons prepared from lignin by chemical activation," *Carbon* 40(4), 630-632.

Hirose, T., Zhao, B., Okabe, T., and Yoshimura, M. (2002). "Effect of carbonization temperature on the basic properties of woodceramics made from carbonized bamboo fiber and liquefied wood," *Journal of Materials Science* 37(16), 3453-3458.

Ishii, C., Suzuki, T., Shindo, N., and Kaneko, K. (1997). "Structural characterization of heat-treated activated carbon fibers," *Journal of Porous Materials* 4(3), 181-186.

Lastoskie, C., Gubbins, K. E., and Quirke, N. (1993). "Pore size distribution analysis of microporous carbons: A density functional theory approach," *The Journal of Physical Chemistry* 97(18), 4786-4796.

Lee, J. G., Kim, J. Y., and Kim, S. H. (2006). "Microtexture and electrical properties of PAN-ACF," *Journal of Materials Science* 42(7), 2486-2491.

Ma, X., and Zhao, G. (2008). "Structure and performance of fibers prepared from liquefied wood in phenol," *Fibers and Polymers* 9(4), 405-409.

Ma, X., and Zhao, G. (2011). "Variations in the microstructure of carbon fibers prepared from liquefied wood during carbonization," *Journal of Applied Polymer Science* 121(6), 3525-3530.

Mangun, C. L., Benak, K. R., Economy, J., and Foster, K. L. (2001). "Surface chemistry, pore sizes and adsorption properties of activated carbon fibers and precursors treated with ammonia," *Carbon* 39(12), 1809-1820.

Polovina, M., Babi, B., Kaluderovi, B., and Dekanski, A. (1997). "Surface characterization of oxidized activated carbon cloth," *Carbon* 35(8), 1047-1052.

Ryu, Z., Rong, H., Zheng, J., Wang, M., and Zhang, B. (2002). "Microstructure and chemical analysis of PAN-based activated carbon fibers prepared by different activation methods," *Carbon* 40(7), 1144-1147.

Shen, W., Guo, Q., Zhang, Y., Liu, Y., Zheng, J., Cheng, J., and Fan, J. (2006). "The effect of activated carbon fiber structure and loaded copper, cobalt, silver on the adsorption of dichloroethylene," *Colloids and Surfaces A: Physicochemical and Engineering Aspects* 273, 147-153.

Su, C., Zeng, Z., Peng, C., and Lu, C. (2012). "Effect of temperature and activators on the characteristics of activated carbon fibers prepared from viscose-rayon knitted fabrics," *Fibers and Polymers* 13(1), 21-27.

Uraki, Y., Nakatani, A., Kubo, S., and Sano, Y. (2001). "Preparation of activated carbon fibers with large specific surface area from softwood acetic acid lignin," *Journal of Wood Science* 47(6), 465-469.

Wang, R., Li, W., and Liu, S. (2012). "A porous carbon foam prepared from liquefied birch sawdust," *Journal of Materials Science* 47(4), 1977-1984.

Xiaojun, M., and Guangjie, Z. (2010). "Preparation of carbon fibers from liquefied wood," *Wood Science and Technology* 44(1), 3-11.

Xu, C., and Etcheverry, T. (2008). "Hydro-liquefaction of woody biomass in sub- and super-critical ethanol with iron-based catalysts," *Fuel* 87(3), 335-345.

Article submitted: July 17, 2012; Peer review completed: September 15, 2012; Revised version received: September 21, 2012; Accepted: September 24, 2012; Published: September 26, 2012.